Modelling of multipurpose spintronic devices

Thomas Windbacher*, Joydeep Ghosh,
Alexander Makarov, Viktor Sverdlov
and Siegfried Selberherr

Institute for Microelectronics, TU Wien,
Gußhausstraße 27–29/E360,
A-1040 Vienna, Austria
Email: windbacher@iue.tuwien.ac.at
Email: ghosh@iue.tuwien.ac.at
Email: makarov@iue.tuwien.ac.at
Email: sverdlov@iue.tuwien.ac.at
Email: selberherr@iue.tuwien.ac.at
*Corresponding author

Abstract: Modelling of spin transport and spin dynamics, as a prerequisite for designing spintronic devices, is considered. Spin injection into a semiconductor under charge depletion, charge neutrality, and charge accumulation is investigated. The existence of a maximum spin current density in the bulk at a large spin current density at the interface in charge accumulation is related to the spin current at the charge neutrality condition. Then, a novel multipurpose spintronic device is proposed and its structure as well as its working principle is explained. Two important applications for this structure, a flip flop and a nano-scale oscillator, are further elucidated and the properties related to these applications are investigated.

Keywords: spin drift diffusion; spin injection; spin transport; spin threshold current; spin transfer torque; flip flop; latch; bias-field free nano-oscillator; multipurpose spintronic device; large scale integration.

Reference to this paper should be made as follows: Windbacher, T., Ghosh, J., Makarov, A., Sverdlov, V. and Selberherr, S. (2015) 'Modelling of multipurpose spintronic devices', *Int. J. Nanotechnol.*, Vol. 12, Nos. 3/4, pp.313–331.

Biographical notes: Thomas Windbacher studied physics at the Technische Universität Wien, where he received the degree of Diplomingenieur in October 2006. He joined the Institute for Microelectronics in October 2006 and finished his doctoral degree on engineering gate stacks for field-effect transistors in 2010. From 2010 until the beginning of 2012 he worked as a patent attorney candidate in Leoben. In March 2012, he rejoined the Institute for Microelectronics, where he currently works on the modelling and simulation of magnetic device structures.

Joydeep Ghosh studied Electrical Engineering (bachelors) at the Jadavpur University, Kolkata. He was in IT industry for three years. Then he studied 'Micro-nano science' (master's) at the Technical University of Chemnitz, Germany, where he completed his studies in 2011. He joined the Institute for Microelectronics in March 2012. His current scientific interests include the drift diffusion equation with spin relaxation in silicon based semiconductor devices.

Copyright © 2015 Inderscience Enterprises Ltd.

Alexander Makarov studied information technology at the Volgograd State Technical University, where he received the BSc in 2006 and MSc in 2008. He joined the Institute for Microelectronics in October 2009 and has obtained the doctoral degree in March 2014. He is currently employed as a post-doc researcher. His scientific interests include Monte-Carlo simulations and non-volatile memory device modelling.

Viktor Sverdlov received his Master of Science and PhD in Physics from the State University of St.Petersburg, Russia, in 1985 and 1989, respectively. From 1989 to 1999 he worked as a staff research scientist at the V.A.Fock Institute of Physics, St.Petersburg State University. During this time, he visited ICTP (Italy, 1993), the University of Geneva (Switzerland, 1993–1994), the University of Oulu (Finland,1995), the Helsinki University of Technology (Finland, 1996, 1998), the Free University of Berlin (Germany, 1997), and NORDITA (Denmark, 1998). In 1999, he became a staff research scientist at the State University of New York at Stony Brook. He joined the Institute for Microelectronics, Technische Universität Wien, in 2004. His scientific interests include device simulations, computational physics, solid-state physics, and nanoelectronics.

Siegfried Selberherr received the degree of Diplomingenieur in electrical engineering and the doctoral degree in technical sciences from the Technische Universität Wien in 1978 and 1981, respectively. He has been holding the venia docendi on Computer-Aided Design since 1984. From 1988 to 1999 he was the Head of the Institute for Microelectronics. From 1998 to 2005 he served as Dean of the Faculty of Electrical Engineering and Information Technology. His current research topics are modelling and simulation of problems for microelectronics engineering.

This paper is a revised and expanded version of a paper entitled ‘Modeling spin-based electronic devices’ presented at *Nano and Giga Challenges in Microelectronics (NGCM)*, Phoenix, USA, 10–14 March, 2014.

1 Introduction

Owing to the continuous demand for cheap electronics with increased performance, CMOS scaling became the key to stay competitive on the semiconductor market. The ITRS [1] offers a commonly accepted guideline for a collective effort to the upcoming technology generations. Owing to the struggle to keep control over the channel in CMOS devices when scaling them down, new processes, materials, and device structures were introduced, e.g., local and global strain techniques, high-k/metal gates, and Tri-gate FETs. In parallel the static power consumption growth and the interconnection delay increase started to become a significant obstacle for scaling [2]. A viable way to eliminate the static power loss is to cut off unused circuit parts from their power supply. However, this transition from permanently ‘On’ circuits to normally ‘Off’ circuits requires the introduction of non-volatility. The use of non-volatile elements, which do not need any energy supply to keep their state, is paramount for the successful implementation of this new type of information processing. Here, spin as a degree of freedom gains much attention. Spin-based devices are non-volatile and are characterised by fast operation and high endurance [3]. Additionally, they not only enable efficient information storage but also change the way information is processed and

transferred between circuit blocks [4,5]. This shift away from the Von Neumann architecture is promising, because it allows to avoid the nowadays performance limiting information transport between the storage and the computation unit over a common bus.

The most straightforward and by now commercially available application of non-volatile spintronic devices is as a supplement or even replacement for static and dynamic CMOS-based memory [6,7]. The development started with the introduction of the giant magnetoresistance (GMR) [8,9] and was further bolstered by the discovery of the tunneling magnetoresistance (TMR) effect [10], which led to an improved performance of magnetic-based memories and brought them to commercialisation [11,12]. Initially, the developed magnetic random access memories (MRAM) required a magnetic field to write the logic state in the memory cells [11,13]. This caused the need for an extra current carrying wire for the writing field generation and was accompanied by high writing energies as well as unfavourable scaling behaviour, which made the first generation of MRAM very disadvantageous for use in large scale integration applications. The theoretical prediction [14,15] and the experimental proof [16,17] of the spin transfer torque (STT) effect abolished the writing wire limitation by enabling purely electrically controlled switching of magnetic layers. Nevertheless, there are still challenges to overcome, like the up to now still rather high current required to switch the magnetisation orientation of the free magnetic layer and the decreasing thermal stability when the magnetic tunnel junctions (MTJ) are shrunk. Even though the introduction of perpendicular magnetic anisotropies in combination with magnesium oxide tunnel barriers reduced the switching energy to a level, where it is able to compete with CMOS SRAM cache [18–21], the CMOS logic transistors outperform MTJ devices with respect to switching energy [3]. However, the MTJ-based memory technology is superior with respect to static power loss and mature enough to encourage the introduction of STT-based MRAM products [7,22–24].

Owing to the excellence, experience, and vast knowledge related to silicon and CMOS technology, it is very attractive to introduce spintronic silicon devices by first supplementing and later partly replacing CMOS devices and circuits. This requires the integration of spintronic devices together with MOSFETS on the same chip. Additionally, silicon possesses features favouring for a long spin lifetime, e.g., a weak spin-orbit interaction and zero spin for ^{28}Si isotope nuclei, which makes it extremely attractive for spin-driven applications. Recent outstanding advances in essential spin-related properties needed for implementing spintronic devices such as injection of spin-polarised currents into silicon, spin transport, spin manipulation, and detection have been demonstrated [25,26]. Therefore, the understanding of spin injection and spin transport in silicon is a key for novel spin-driven devices and will be discussed in the following section.

2 Modelling spin transport in silicon

Even though spin injection, detection, and the spin transport in silicon at room temperature have been demonstrated, thus promising advantageous performance, several observations are still lacking an explanation within the theories. For instance, there is an unrealistically high amplitude of the voltage signal related to the spin accumulation in silicon for a three-terminal spin injection/detection scheme [26]. Recently, a possible way to explain this behaviour by resonant tunelling was suggested [27]. Also the influence of a high electric field on the spin transport in semiconductors and the accompanied boost in magnetoresistance could be responsible [28]. Another explanation, indicating that the spin injection signal can

be boosted by an order of magnitude, is to take properly into account space-charge effects at the interface [29]. Later the existence of an upper threshold spin current injectable into a semiconductor was predicted [30]. It was not clear, however, what determines the value of the maximum current and whether it can explain the discrepancy between the observed spin accumulation signal [26] and the theory [31,32]. This discrepancy motivated us to study charge accumulation as well as depletion at the spin injection boundary.

The employed spin drift-diffusion model successfully describes the classical transport of charge carriers and their respective spins in a semiconductor. The expression for the current density $J_{\uparrow(\downarrow)}$, carried by the electrons with spin up(down), is given by [33]:

$$J_{\uparrow(\downarrow)} = e\, n_{\uparrow(\downarrow)}\, \mu\, E + e\, D\, \nabla n_{\uparrow(\downarrow)}, \tag{1}$$

where D is the electron diffusion coefficient, μ is the electron mobility, E denotes the electric field, and e is absolute value of the electron charge. The spin concentration is expressed as $n_\uparrow(n_\downarrow)$, respectively. The electron concentration is thus given by $n = n_\uparrow + n_\downarrow$ and the spin density can be defined as $s = n_\uparrow - n_\downarrow$. The electron charge (spin) current is determined analogously to the corresponding densities $J_c(J_s) = J_\uparrow \pm J_\downarrow$. Furthermore, the spin polarisation is given as $P = \dfrac{s}{n}$. Inserting the definitions from (1) into the steady-state continuity equation and adding spin scattering leads to [33]:

$$\nabla \cdot J_{\uparrow(\downarrow)} = \pm e \left(\frac{n_\uparrow - n_\downarrow}{\tau_s} \right), \tag{2}$$

where τ_s is the spin relaxation time. The same procedure performed with the Poisson equation is used to define the electric field:

$$\nabla \cdot E = e\, \frac{n_\uparrow + n_\downarrow - N_D}{\epsilon_{Si}}, \tag{3}$$

where ϵ_{Si} is the electric permittivity of silicon and N_D is the doping concentration. V_{th} denotes the thermal voltage: $V_{th} = \frac{k_B\, T}{q}$, where k_B is the Boltzmann constant and T is the temperature. The intrinsic spin diffusion length is defined as $L = \sqrt{D\tau_s}$ and the diffusion coefficient D is related to the mobility by the Einstein relation $D = \mu\, V_{th}$. The respective charge current and the spin currents are:

$$J_c = e\, n\, \mu\, E + e\, D\, \frac{\mathrm{d}n}{\mathrm{d}x}, \tag{4}$$

$$J_s = e\, s\, \mu\, E + e\, D\, \frac{\mathrm{d}s}{\mathrm{d}x}. \tag{5}$$

The spin density equation is given by:

$$\frac{\mathrm{d}^2 s}{\mathrm{d}x^2} + \left(\frac{1}{V_{th}} \right) \frac{\mathrm{d}}{\mathrm{d}x}(Es) - \frac{s}{L^2} = 0\,, \tag{6}$$

where both s and E are position dependent.

In order to study the spin injection into silicon one has to define boundary conditions. For simplicity we consider the case of complete spin polarisation at the interface. Since the

spins' chemical potentials in a semiconductor are related to their concentration [33], we define the boundary conditions as follows:

$$\begin{bmatrix} n_\uparrow^0 \\ n_\downarrow^0 \end{bmatrix} = N_D \begin{bmatrix} \exp(\frac{\mu_{\text{Chem}}}{V_{th}}) \\ 0 \end{bmatrix} . \tag{7}$$

μ_{Chem} defines the charge chemical potential. This equation allows to inject (release) only up-spin and hence charge at the same time. Therefore, (7) can describe: spin injection at charge neutrality ($\mu_{\text{Chem}} = 0$), spin injection at charge accumulation ($\mu_{\text{Chem}} > 0$), and spin injection at charge depletion ($\mu_{\text{Chem}} < 0$).

In order to investigate how far the spin density from a single interface is able to penetrate into the silicon bar under varying conditions, the second boundary is positioned at a distance of several times the spin diffusion length ($\geq 3L$) and the spin density s is set to 0. Simulations were performed for an n-doped silicon bar with an intrinsic spin diffusion length of $L = 1\ \mu\text{m}$, a bar length of several microns, a doping concentration of $N_D = 10^{16}\ \text{cm}^{-3}$, and an electron mobility of $1400\,\text{cm}^2\text{V}^{-1}\text{s}^{-1}$. The potential U is applied at the right boundary and the left boundary is grounded. Therefore, the charge current may flow left or right depending on the sign of U, while the spin flow, owing to the injection at the left side, heads towards the right side.

By employing (7) and varying the chemical potential μ_{Chem} as well as the applied potential U it is possible to tune the spin (charge) accumulation and the spin (charge) current densities. The results for the spin density and the spin current densities along the bar are obtained at a fixed current density of $11.9\ \text{MA/m}^2$ (see Figures 1 and 2). It is also demonstrated that the threshold spin current in the bulk is controlled by the spin current value injected under charge neutrality conditions, provided that the spin polarisation at the interface and the charge current through the system are fixed. Therefore, spin injection through the accumulation layer can boost the spin current only within the screening length from the interface, while the spin current in the bulk is determined by the spin injection at the charge neutrality condition (provided the spin diffusion length is much larger than the screening length). Under depletion the spin current is suppressed owing to the fact that the minority spin drift and diffusion currents flow towards the injection interface thus reducing the net spin current.

Figure 1 Spin density as a function of the interface distance for depletion ($\mu_{\text{Chem}} = -100\ \text{mV}$), charge neutrality ($\mu_{\text{Chem}} = 0\ \text{mV}$), and accumulation ($\mu_{\text{Chem}} = 100\ \text{mV}$). The charge current density is fixed by adjusting the voltage U (see online version for colours)

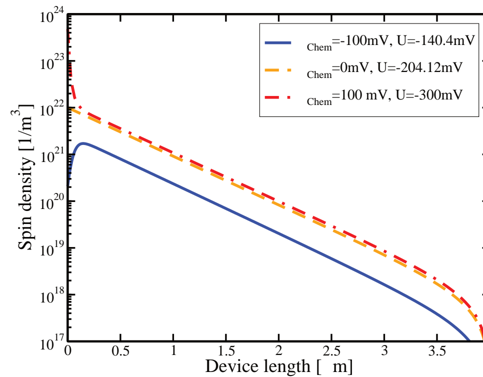

Figure 2 Spin current density as a function of the interface distance for depletion, charge neutrality, and accumulation (conditions as in Figure 1). The spin current density shows a significant drop for depletion, while under accumulation it relaxes to the charge neutrality curve (see online version for colours)

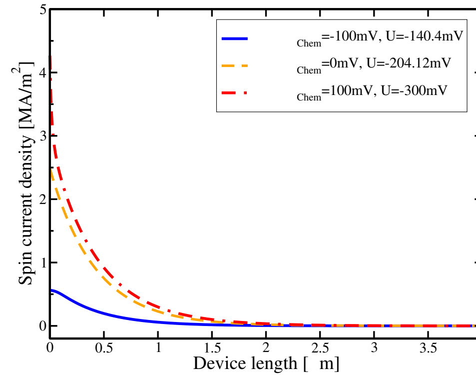

3 Multipurpose spintronic devices

As stated in the introduction the seemingly endless demand for fast and cheap (consumer) electronics has propelled the scaling efforts since the very beginnings of CMOS. Currently, the miniaturisation level reached a stage where the upcoming technology nodes require to handle fundamental physical limitations as well as soaring factory costs. Therefore, the search for alternative materials and devices capable of pushing the scaling limits and power efficient computing gains momentum. Usually digital integrated circuits are associated with memory and combinatorial logic applications. However, there is another essential building block for information processing – namely sequential logic. The logic state of sequential logic not only depends on its current inputs, but also on its input history [34]. Flip flops as well as latches belong to this group of logic. Several circuit designs have been proposed to exploit non-volatility and are commonly based on CMOS-MTJ hybrid solutions [35]. While the non-volatility is introduced by MTJs, the actual computation is carried out by CMOS circuits. Thus, the MTJs act solely as memory and every time information is written or read the signal mismatch between the CMOS circuits and the MTJs has to be bridged. This requires additional CMOS (sense) amplifiers and results rather in an integration density decrease than a denser layout.

Therefore, we proposed a non-volatile magnetic flip flop which handles the computation as well in the magnetic domain [36,37]. This enables the creation of denser layouts as well as to harvest the beneficial features related to spintronics.

3.1 Device structure

Before further advancing into the modelling of the multipurpose structure one has to elucidate the basic assumptions and prerequisites used. The non-volatile multipurpose device structure comprises three fixed anti-ferromagnetically polariser stacks with perpendicular (parallel to the z-axis) magnetisation orientation (see Figure 3). Two of the polariser stacks are used for input (A and B) and one polariser stack Q is used for read out. Owing to the antiferromagnetic configuration of the polariser stacks it is presumed that the stray fields of the stacks are small enough to be ignored. All three polariser stacks are

connected to a shared free magnetic layer, with a constant perpendicular uni-axial anisotropy described by K_1, by means of a non-magnetic layer, e.g., Cu, MgO, Al_2O_3. It is also assumed that the free layer exhibits a width of $w_0 = 30$ nm, a length of $l_0 = 120$ nm, and a thickness of $t_0 = 3$ nm. The width of the device is aligned along the x-axis, the length along the y-axis, and the thickness along the z-axis. Furthermore, the device is operated via voltage/current pulses and the polarity of the pulses is mapped to logic '0' for negative pulses and '1' for positive pulses, respectively. Applying a positive voltage to one of the terminals and assuming a grounded metal layer attached to the bottom of the shared free layer will cause a current flowing from the contacts (A,B,Q) through the free layer which is defined as positive (against z-axis) and the corresponding electron flow is oriented along the opposite direction (positive z-axis).

Figure 3 The basic structure of the multipurpose device. Two polariser stacks (A and B) are employed for input. The polariser stack Q is used for read out. All three stacks are built out of anti-ferromagnetically coupled perpendicularly oriented stacks and are connected by a non-magnetic layer to their common free layer with a perpendicular anisotropy (see online version for colours)

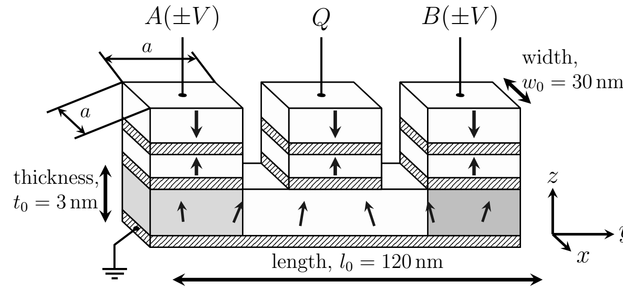

The information is stored by the magnetisation orientation of the shared free layer and is read out either by employing the GMR or the TMR effect.

In the following the switching time is defined as the time it takes for the magnetisation of the free layer to reach 80% of its final state.

One has to note that the proposed device structure has a resamblance with the spin torque majority gate [38]. But while the majority gate requires three inputs to avoid a tie between the acting torques and the related unclear output state for evenly split inputs, the flip flop rests upon exactly two inputs to exploit the tie input combinations for realising its HOLD operation. Therefore, the flip flop can be operated without losing its initial information in contrast to the majority gate which loses its old state everytime it is operated.

3.2 Models

The investigated magnetic device structures are well covered by the Landau-Lifshitz-Gilbert equation [39,40] supplemented with an STT term $\vec{T}$:

$$\frac{\mathrm{d}}{\mathrm{d}t}\vec{m} = \gamma\left(-\vec{m}\times\vec{H}_{\mathrm{eff}} + \alpha\left(\vec{m}\times\frac{\mathrm{d}}{\mathrm{d}t}\vec{m}\right) + \vec{T}\right) \tag{8}$$

$\vec{m}$ denotes the reduced magnetisation, $\gamma = 2.211\times10^5$ m/As the electron gyromagnetic ratio, α the dimensionless damping constant, and $\vec{H}_{\mathrm{eff}}$ the effective field in A/m.

The first term in (8) describes the precessional motion due to the effective magnetic field $\vec{H}_{\text{eff}}$. The second term introduces a power dissipation proportional to $\dot{\vec{m}}$ and the last term describes the torque acting on the local magnetisation due to the electron spin polarisation when they pass the free magnetic layer. Depending on the non-magnetic layer the spin transfer torque $\vec{T}$ has to be modelled either by [41] (Oxides, MTJs) or by the following expression [42] (metal, spin valve):

$$\vec{T} = \frac{\hbar}{\mu_0 e} \frac{J}{l M_S} \frac{P \Lambda^2}{(\Lambda^2 + 1) + (\Lambda^2 - 1)\, \vec{m} \cdot \vec{p}} \cdot \\ \cdot (\vec{m} \times \vec{p} \times \vec{m} - \epsilon' \vec{m} \times \vec{p}) \tag{9}$$

$\hbar$ denotes the Planck constant, μ_0 the permittivity of vacuum, J the applied current density, l the free layer thickness, M_S the magnetisation saturation, P the polarisation, $\vec{p}$ the unit polarisation direction of the polarised current, and Λ a fitting parameter handling non-idealities. Both STT models, for the spin valve (later employed) and the model for an MTJ, exhibit an in-plane ($\vec{m} \times \vec{p} \times \vec{m}$) and an out-of-plane component ($\vec{m} \times \vec{p}$). But while in MTJs the out-of-plane component is non-negligible [43,44], in spin valves the contribution is only small [45]. In the case of two magnetic interfaces (penta layer structure) the total spin transfer torque is calculated as the sum of the corresponding spin torque interface contributions.

The effective field $\vec{H}_{\text{eff}}$ is calculated as the functional derivative of the free energy density containing uni-axial anisotropy, exchange, and demagnetisation contributions [46].

3.3 Flip flop

If a positive current pulse is applied to one of the polariser stacks (A or B) of the multipurpose structure, the electrons flow from the shared free layer towards the non-magnetic layer (see Figure 1). Depending on the electrons' spin orientation the electrons pass easily into the polariser stack (parallel oriented to polariser) or they get flipped. This leads to a local (beneath the polariser stack) surplus of unaligned spins. These spins relax to the local magnetisation orientation and excite precessions in the shared free layer's magnetisation orientation. The precessions spread through the free magnetic layer owing to magnetic exchange exciting precessional motions in the whole free layer [47]. During the excitation precessions in the whole free layer start to build up, until they eventually pass the energy barrier between the two stable magnetisation states and the system relaxes in the other stable state. If now, instead of one, two synchronous pulses are applied to the inputs A and B, two spin torques act on the free layer's magnetisation. Depending on the polarity of the input pulses (cf. (9)), the two torques either superimpose constructively speeding up the magnetisation flip or work against each other damping the switching of the free layer's magnetisation.

Two inputs allow four input combinations. Assuming two negative input pulses both generated torques will strive to align the free layer's magnetisation parallel to the z-axis and the free layer's magnetisation will stay unchanged. On the contrary for two positive pulses both torques will try to align the free layer's magnetisation anti-parallel to the z-axis and the free layer will switch faster, than in the case of a single input pulse. If the input pulses possess opposing polarities, there will be always one torque pushing towards the positive z-axis, while the other will push towards the anti-parallel orientation. This way they compensate each other and the magnetisation orientation stays unchanged. Mapping this behaviour to a logic table shows that for two sufficiently long and strong identical pulses

($A = B = 0$ or $A = B = 1$) '0' (antiparallel layers, high resistance state (HRS)) and '1' (parallel layers, low resistance state (LRS)) can be written into the free layer, while for two opposing pulses the initial state is held ($A \neq B \rightarrow Q(i) = Q(i-1)$). This perfectly fits to the definition of sequential logic, in particular, this is exactly what is required for flip flop logic [34]. Two positive pulses ('1') correspond to the SET ($Q \rightarrow 1$) operation, while two negative pulses ('0') perform the RESET ($Q \rightarrow 0$) operation.

Figure 4 shows the switching time for the flip flop's SET/RESET operation (two identical pulses) as a function of current density (see Table 1 and [36]). In analogy to a single MTJ stack the flip flop starts to flip its magnetisation orientation at a certain threshold current density and further increasing the current density leads to a steep decrease in switching times. On the other hand, the HOLD operation (opposing pulses) demands that the free layer's magnetisation does not change as depicted in Figure 5. This holds true up to 4×10^{11} $\mathrm{A/m^2}$, where the damping is not sufficient anymore and oscillations in the free layer are excited. One has to mention that the sharp drop in switching time at 4×10^{12} $\mathrm{A/m^2}$ does not mean that the flip flop holds its state again, but instead the torque becomes so strong that the magnetisation flips without extensive precessional motions.

Figure 4 Switching time for the flip flop's SET and RESET operation (two identical pulses) as a function of current density. The dashed line at 7×10^{10} $\mathrm{A/m^2}$ marks the bias point for the layer variations shown in Figures 6–8 (see online version for colours)

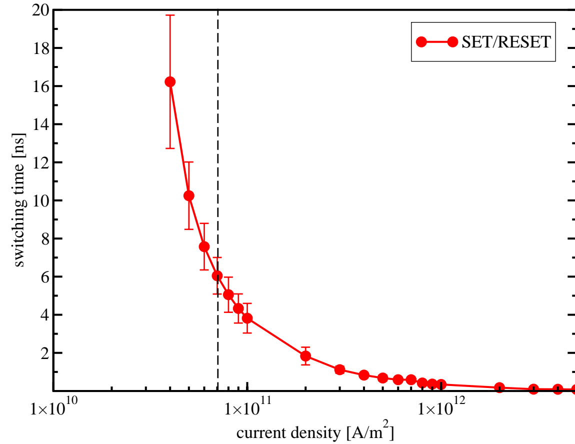

The proposed flip flop is capable of tolerating relatively large static normal-distributed field variations [48]. Figure 6 depicts three operations of the flip flop. For all three cases a normal-distributed constant external magnetic field with zero mean and variable distribution width was added to test the devices' ability to tolerate disturbances:

$$H_{i,\mathrm{rand}} = \xi_i \, M_S \, s, \quad \mathrm{i} \in \{\mathrm{x}, \mathrm{y}, \mathrm{z}\}, \tag{10}$$

$$\langle \xi_i, \xi_j \rangle = \delta_{i,j}, \langle \xi_\mathrm{i} \rangle = 0, \text{ and } \langle \xi_\mathrm{i}^2 \rangle = 1. \tag{11}$$

s denotes the disturbance strength and ξ_i the normal-distributed random variable. 101 random field realisations for each disturbance strength s were simulated to allow for statistical analysis. The initial free layer magnetisation was set close to its upper equilibrium position for all three cases. The STANDBY operation was simulated without arbitrary STT

to test the free layer's capability to hold its current state. Above $\approx 0.5M_S$ disturbance strength s the structure starts to relax in the opposite direction for STANDBY and hence fails. The HOLD operation works at least until 20% of M_S and the SET/RESET operation until $\approx 50\%$ of M_S for the parameters given in Table 1.

Table 1 Parameters used for the simulations

Parameter	*Value*
Free layer length l_0	120 nm
Free layer width w_0	30 nm
Free layer thickness t_0	3 nm
Contact sizes a	$(30 \text{ nm})^2$
Magnetisation saturation M_S	4×10^5 A/m
Out-of-plane uni-axial anisotropy K_1	10^5 J/m^3
Uniform exchange constant A_{exch}	2×10^{-11} J/m
Polarisation P	0.3
Non-magnetic layer	Cu
Gilbert gyromagnetic ratio γ	2.211×10^5 m/As
Damping constant α	0.01
Non-adiabatic contribution ϵ'	0.1 [38]
Λ	2
Discretisation length Δx,Δy	2 nm
Discretisation length Δz	3 nm
Discretisation time Δt	2×10^{-14} s

Figure 5 Switching time for the flip flop's HOLD operation (two opposing pulses) as a function of current density. The dashed line at 10^{12} A/m^2 marks the bias point for the layer variations shown in Figures 9–11 (see online version for colours)

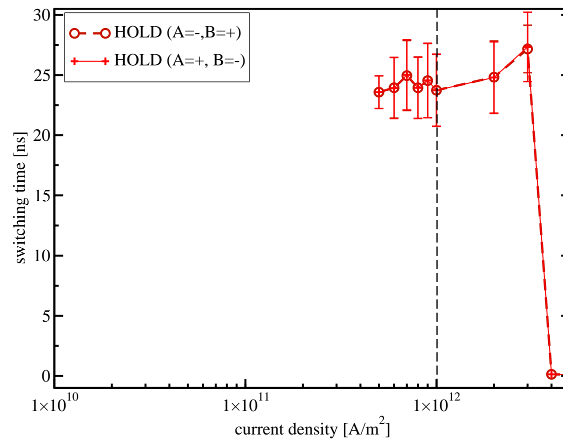

Flip flops are commonly utilised in time critical applications and operated with clocked signals. Therefore, it is essential to understand and to control their switching behaviour. Again the parameters from Table 1 are employed, the current density was fixed for both

inputs at 7×10^{10} A/m^2 and the free layer's (initial) dimensions were varied in length (60–200 nm), width (20–70 nm), and thickness (1–4 nm), independently.

Figures 7 and 8 show that changing the free layer's thickness and length has a significant influence on the switching time. On the other hand, changes in the width cause only marginal shifts in the switching time (see inset of Figure 8). This behaviour is related to the switching time by the thermal stability barrier relationship $t \propto \exp(E/k_BT)$ [49]. The thermal stability barrier E is proportional to the net anisotropy (perpendicular anisotropy minus shape anisotropy [50]) times volume. In the precessional switching regime the switching time is determined by the thermal stability barrier [49]. Thus, changes in the geometry like length, width, thickness, and volume directly translate to shifts in the switching time through the changes in the minimum energy barrier separating the two stable states. While for the longer (thicker) layers the shape anisotropy contribution is mostly saturated and the linear volume dependence dominates, for smaller layer length (thickness) the shape anisotropy contribution starts to increase (decrease) the switching barrier and leads to deviations from the linear volume dependence (see Figures 7 and 8). Therefore, the free layer thickness is the most critical parameter determining the switching time, followed by the layer length.

Figure 6 The STANDBY operations were set up without any pulse, while the HOLD and SET/RESET operations were carried out with opposing and identical pulses, respectively. Each point represents the switching probability for 101 samples (see online version for colours)

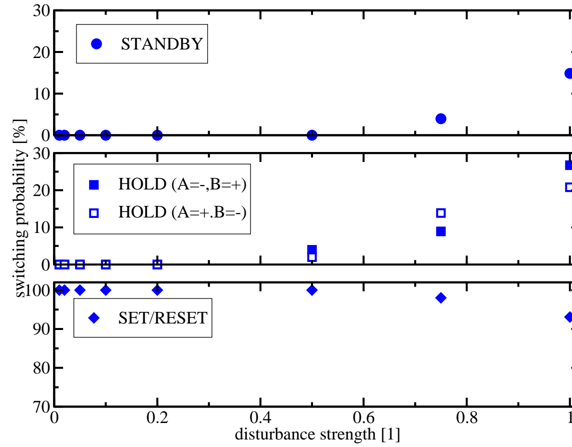

Figure 8 shows the logarithmised switching time as a function of the free layer thickness. One can immediately see that the free layer thickness has a pronounced influence on the switching time (from $1\ \mathrm{nm} \rightarrow 1.5\ \mathrm{ns}$ to $4\ \mathrm{nm} \rightarrow 11.9\ \mathrm{ns}$). It can also be observed that for thicker films the linear fit matches very well (linear fit $\rightarrow$ dashed line, simulation data $\rightarrow$ solid line), while for a thickness below $2\ \mathrm{nm}$ a shorter switching time than predicted by the linear fit is found. In order to explain this behaviour we assume the exponential dependence of the switching time $t \propto \exp(E/k_BT)$ [49] on the thermal stability barrier E described by [51]:

$$E = \mu_0/2\, M_S\, V\, (H_{\mathrm{K}_1} - 4\pi N_z M_S). \tag{12}$$

Figure 7 Logarithmised switching time as a function of free layer length. The dashed line describes the linear energy dependence on the free layer volume (area is fixed). The full line shows our simulation results and deviations due to the shape anisotropy change (see online version for colours)

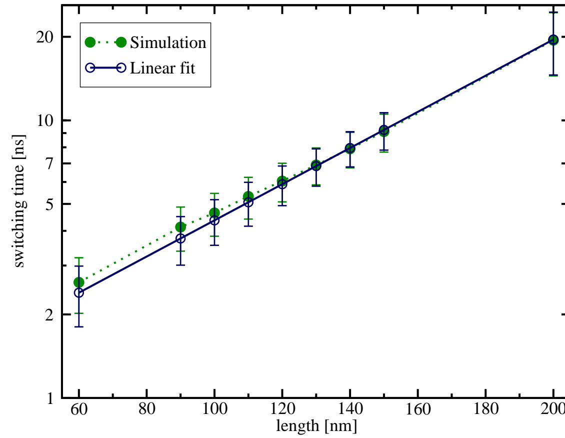

Figure 8 Logarithmised switching time as a function of free layer thickness. The dashed line shows the linear volume dependence, while the full line depicts our simulation results taking shape anisotropy effects into account. The bars depict the width of the distribution ($\pm 3\sigma$) (see online version for colours)

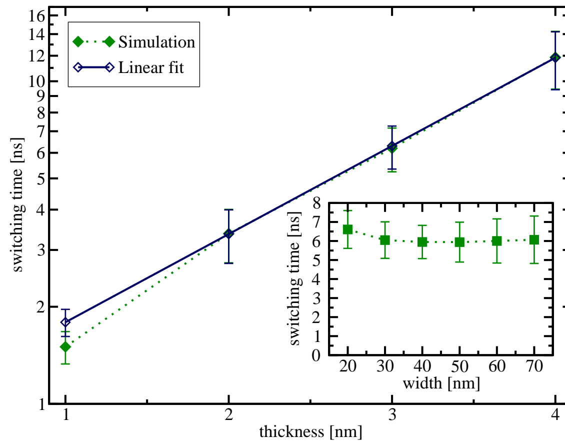

Here, μ_0 denotes the magnetic permeability, V describes the free layer volume, H_{K_1} the uni-axial anisotropy field, and N_z the demagnetisation factor along the z-axis.

The linear behaviour for the thicker free layers is consistent with a saturated demagnetisation factor N_z and the linearly growing volume when increasing the layer thickness [51]. On the other hand for thinner free layers the demagnetisation factor is not saturated as compared to thick layers and starts to grow when the thickness is decreased. Thus, the difference between the fixed uni-axial anisotropy field H_{K_1} and the growing shape anisotropy [50] becomes smaller which lowers the switching barrier leading to a shorter switching time.

For changing the free layer width (shown in Figure 8 as inset) the linear volume change is compensated by the linear contact width change and, therefore, the dependence is nearly constant, until the shape anisotropy contribution starts to change significantly and raises the switching barrier (from $20\ \mathrm{nm} \rightarrow 6.6\ \mathrm{ns}$ to $70\ \mathrm{nm} \rightarrow 6\ \mathrm{ns}$).

The opposite trend shown in Figure 7 is observed, when the dependence of the switching time on the free layer length is investigated (from $60\ \mathrm{nm} \rightarrow 2.6\ \mathrm{ns}$ to $200\ \mathrm{nm} \rightarrow 19.4\ \mathrm{ns}$). This is caused by the reduction of N_z for shorter lengths.

3.4 Nano-oscillators

Oscillators belong to the group of fundamental building blocks and are ubiquitous in modern electronics. They are used in measurement, navigation, communication systems, etc. The periodicity of their output signals is employed for clocking digital circuits, generating electromagnetic waves, as a reference source for system synchronisation, and much more. Owing to their nano-scale size, frequency tunability, CMOS compatibility, and broad temperature operation range, spin torque nano-oscillators are very promising as cost effective on-chip integrated microwave oscillators [52].

The presented structure behaves like a flip flop, however, if one now looks at Figure 5 at the current density of $10^{12}\ \mathrm{A/m^2}$, where the flip flop's HOLD operation fails, and one plots the averaged normalised magnetisation orientation $<m_x(t)>$, $<m_y(t)>$, and $<m_z(t)>$ (as shown in Figure 9), one immediately recognises stable and large orbits of precessional motion. The depicted orbits vary with the free layer's dimensions and can also be tuned by changing the applied current densities [53]. The device structure and excitation principle differ from the spin torque nano-oscillators described in Berkov and Miltat [54]. Here, to achieve high frequency oscillations without external magnetic field, we employ two torques acting on opposite ends of the free layer in opposite directions. We note that this is precisely the same structure on which the flip flop was built. Therefore, depending on the operating conditions, the same structure can be employed as a flip flop or an oscillator giving an advantage of additional functionality to the same device. The precessions excited at one end propagate via exchange interaction through the free layer, until they hit the other end of the layer, where they are repelled, travel back again, and so on.

Figure 9 Large and stable precessional motions of the free layer as a function of the layer thickness. $<m_x(t)>$, $<m_y(t)>$, and $<m_z(t)>$ denote the averaged and normalised pseudo macros spin components (see online version for colours)

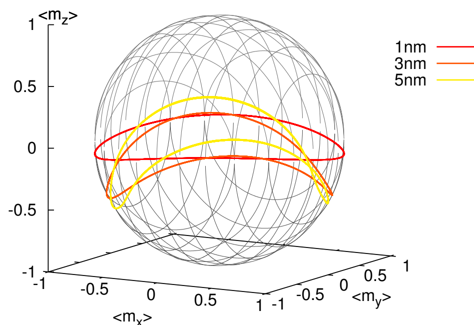

As can be seen in Figure 9 the precessional motion is a superposition of an in-plane oscillation and a periodic out-of-plane movement. The oscillator's frequency can be tuned

by changing the device dimensions. For instance, the longer the free layer the longer it takes for the precessions to travel through the layer and, therefore, the oscillation frequency is decreased (Figure 10). Changing the layer thickness and width also significantly influences the precession frequency (see Figure 11). While width changes cause frequency shifts by a factor of 10 less than those by changing the length, changing the layer thickness causes a big frequency shift. This is due to the increase of the shape anisotropy along the z-direction, when the layer thickness is reduced. As described before the shape anisotropy and the uni-axial out-of-plane anisotropy oppose each other. Therefore, a stronger shape anisotropy weakens the net out-of-plane anisotropy of the free layer, which leads to less vertical oscillation movement and to more pronounced in-plane oscillations for thinner free layers (cf. Figure 9 and [50,55]).

Figure 10 Oscillation frequency as a function of free layer length. The in-plane oscillations are described by $f_{x,y}$ and the out-of-plane movement by f_z (see online version for colours)

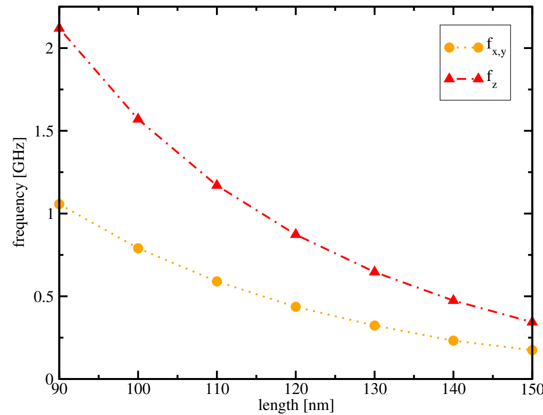

Figure 11 Oscillation frequency as a function of free layer thickness and width (see online version for colours)

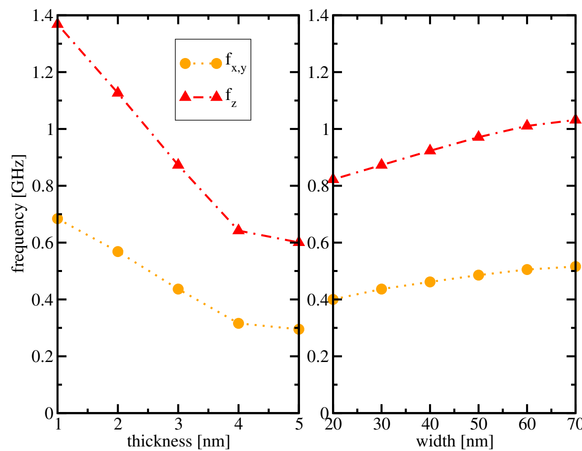

Additionally, the oscillations are not restricted to in-plane and perpendicular magnetisation structures [56]. There are also large and stable oscillations in stacks with in-plane

magnetisation orientation (cf. Figure 12). Changing the anisotropies from out-of-plane to in-plane relocates the oscillations to the yz-plane instead of the xy-plane, as shown in Figure 13.

Figure 12 Alternative structure with in-plane polariser stacks and in-plane free layer magnetisation (see online version for colours)

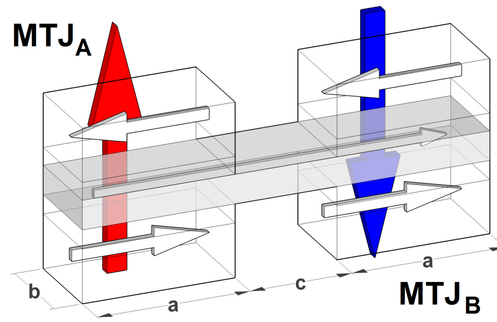

Figure 13 For in-plane polariser stacks and in-plane free layer orientation (cf. Figure 12) the oscillation plane changes from the xy-plane (Figure 9) to the yz-plane (see online version for colours)

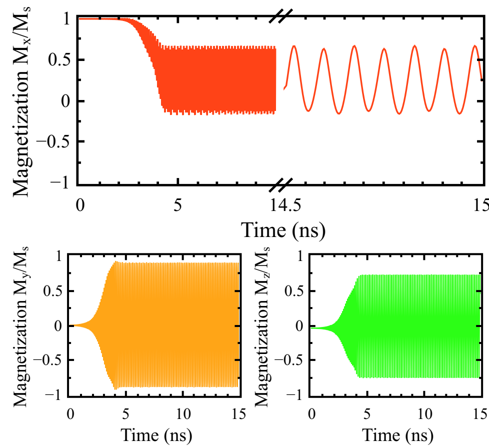

4 Conclusion

Even though the degree of maturity of spintronics vastly varies and there are still many challenges to understand and explore, the up to now gained results and findings are already very promising for future exploitation and application in large scale integration. By modelling the spin injection from a space charge layer we demonstrated that the maximum spin current in the bulk is defined by spin injection at the charge neutrality conditions. The proposed multipurpose magnetic structure is capable of acting as a flip flop and as an oscillator. The flip flop is robust with respect to normal-distributed disturbances and the

switching time can be tuned by the applied current densities as well as by optimising the free layer dimensions. At higher current densities when the HOLD operation fails the oscillatory behaviour of the free layer's magnetisation is observed. The found oscillations are large and stable, do not require an external bias-field, and can be tuned by the applied current densities and the free layer dimensions as well. Additionally, big and stable oscillations can also be gained for in-plane polarisers and an in-plane free layer magnetisation.

Acknowledgements

This work is supported by the European Research Council through the grant #247056 MOSILSPIN.

References and Notes

1 International Technology Roadmap for Semiconductors, Chapter PIDS, 2012, http://www.itrs.net/Links/2012ITRS/Home2012.htm

2 Kim, N., Austin, T., Baauw, D., Mudge, T., Flautner, K., Hu, J. and Irwin, M., Kandemir, M. and Narayanan, V. (2003) 'Leakage current: Moore's law meets static power', *Computer*, Vol. 36, No. 12, pp.68–75.

3 Nikonov, D. and Young, I. (2013) 'Overview of beyond-CMOS devices and a uniform methodology for their benchmarking', *Proceedings of the IEEE*, Vol. 101, No. 12, pp.2498–2533.

4 Mahmoudi, H., Windbacher, T., Sverdlov, V. and Selberherr, S. (2014) 'Reliability-based optimization of spin-transfer torque magnetic tunnel junction implication logic gates', *Adv. Mater. Res.*, Vol. 854, pp.89–95.

5 Mahmoudi, H., Windbacher, T., Sverdlov, V. and Selberherr, S. (2013) 'Implication logic gates using spin-transfer-torque-operated magnetic tunnel junctions for intrinsic logic-in-memory', *Solid-State Electron.*, Vol. 84, pp.191–197.

6 Makarov, A., Sverdlov, V. and Selberherr, S. (2014) 'Emerging Memory technologies: trends, challenges, and modeling methods', *Microelectron. Reliab.*, Vol. 52, No. 4, pp.628–634.

7 Everspin Technologies, January, http://www.everspin.com/spinTorque- MRAM.php

8 Baibich, M.N., Broto, J.M., Fert, A., Van Dau, F.N., Petroff, F., Etienne, P., Creuzet, G., Friederich, A. and Chazelas, J. (1988) 'Giant magnetoresistance of $(001)Fe/(001)Cr$ magnetic superlattices', *Phys. Rev. Lett.*, Vol. 61, November, pp.2472–2475.

9 Binasch, G., Grünberg, P., Saurenbach, F. and Zinn, W. (1989) 'Enhanced magnetoresistance in layered magnetic structures with antiferromagnetic interlayer exchange', *Phys. Rev. B*, Vol. 39, March, pp.4828–4830.

10 Julliere, M. (1975) 'Tunneling between ferromagnetic films', *Phys. Lett. A*, Vol. 54, No. 3, pp.225–226

11 Chappert, C., Fert, A. and Van Dau, F.N. (2007) 'The emergence of spin electronics in data storage', *Nature Mater.*, Vol. 6, November, pp.813–823.

12 Ikeda, S., Hayakawa, J., Ashizawa, Y., Lee, Y.M., Miura, K., Hasegawa, H., Tsunoda, M., Matsukura, F. and Ohno, H. (2008) 'Tunnel magnetoresistance of 604$\%$ at 300K by suppression of Ta diffusion in $CoFeB/MgO/CoFeB$ Pseudo-spin-valves annealed at high temperature', *Appl. Phys. Lett.*, Vol. 93, No. 8.

13 Hosomi, M., Yamagishi, H., Yamamoto, T. Bessho, K., Higo, Y., Yamane, K., Yamada, H., Shoji, M., Hachino, H., Fukumoto, C., Nagao, H. and Kano, H. (2005) 'A novel nonvolatile memory with spin torque transfer magnetization switching: spin-RAM', *Electron Devices Meeting, 2005. IEDM Technical Digest. IEEE International*, pp.459–462.

14 Slonczewski, J. (1996) 'Current-driven excitation of magnetic multilayers', *J. Magn. Magn. Mater.*, Vol. 159, Nos. 1–2, pp.L1–L7.

15 Berger, L. (1996) 'Emission of spin waves by a magnetic multilayer traversed by a current', *Phys. Rev. B*, Vol. 54, October, pp.9353–9358.

16 Moodera, J.S., Kinder, L.R., Wong, T.M. and Meservey, R. (1995) 'Large magnetoresistance at room temperature in Ferromagnetic thin film tunnel junctions', *Phys. Rev. Lett.*, Vol. 74, April, pp.3273–3276.

17 Miyazaki, T. and Tezuka, N. (1995) 'Giant magnetic tunneling effect in $Fe/Al_2O_3/Fe$ junction', *J. Magn. Magn. Mater.*, Vol. 139, No. 3, pp.L231–L234.

18 Ikeda, S., Miura, K., Yamamoto, H., Mizunuma, K., Gan, H.D., Endo, M., Kanai, S., Hayakawa, J., Matsukura, F. and Ohno, H. (2010) 'A perpendicular-anisotropy $CoFeB - MgO$ magnetic tunnel junction', *Nature Mater.*, Vol. 9, September, pp.721–724.

19 Abe, K., Noguchi, H., Kitagawa, E., Shimomura, N., Ito, J. and Fujita, S. (2012) 'Novel hybrid DRAM/MRAM design for reducing power of high performance mobile CPU', *Electron Devices Meeting (IEDM), 2012 IEEE International*, pp.10.5.1–10.5.4.

20 Yoda, H., Fujita, S., Shimomura, N., Kitagawa, E., Abe, K., Nomura, K., Noguchi, H. and Ito, J. (2012) 'Progress of STT-MRAM technology and the effect on normally-off computing systems', *Electron Devices Meeting (IEDM), 2012 IEEE International*, pp.11.3.1–11.3.4.

21 Kitagawa, E., Fujita, S., Nomura, K., Noguchi, H., Abe, K., Ikegami, K., Daibou, T., Kato, Y., Kamata, C., Kashiwada, S., Shimomura, N., Ito, J. and Yoda, H. (2012) 'Impact of ultra low power and fast write operation of advanced perpendicular MTJ on power reduction for high-performance mobile CPU', *Electron Devices Meeting (IEDM), 2012 IEEE International*, pp.29.4.1–29.4.4.

22 Worledge, D., Brown, S.L., Chen, W., Harms, J., Hu, G., Kilaru, R., Kula, W., Lauer, G., Liu, L.Q., Nowak, J., Parkin, S., Pushp, A., Murthy, S., Robertazzi, R.P., Sandhu, G. and Sun, J. (2013) 'Materials advances in perpendicularly magnetized MgO-tunnel junctions for STT-MRAM', *Abstracts of the 58th Annual Conference on Magnetism and Magnetic Materials, Symposium on Materials Advances of Spin-Torque Switched Memory Devices for Silicon Integration*, pp.BA–02.

23 Slaughter, J., Aggarwal, S., Alam, S., Andre, T., Chia, H.J., DeHerrera, M., Deshpande, S., Houssameddine, D., Janesky, J., Mancoff, F.B., Nagel, K., Schneider, M.L., Rizzo, N.D. and Whig, R. (2013) 'Properties of CMOS-integrated magnetic tunnel junction arrays for spin-torque magnetoresistive random access memory', *Abstracts of the 58th Annual Conference on Magnetism and Magnetic Materials, Symposium on Materials Advances of Spin-Torque Switched Memory Devices for Silicon Integration*, pp.BA–01.

24 Thomas, L., Jan, G., Zhu, J., Liu, H., Lee, Y., Le, S., Tong, R., Pi, K., Wang, Y., Zhong, T., Torng, T. and Wang, P. (2013) 'Magnetization dynamics in perpendicular STT-MRAM cells with high spin-torque efficiency and thermal stability', *Abstracts of the 58th Annual Conference on Magnetism and Magnetic Materials, Symposium on Materials Advances of Spin-Torque Switched Memory Devices for Silicon Integration*, pp.BA–03.

25 Huang, B., Monsma, D. and Appelbaum, I. (2007) 'Coherent spin transport through a 350 micron thick silicon wafer', *Phys. Rev. Lett.*, Vol. 99, October, p.177209.

26 Jansen, R. (2012) 'Silicon spintronics', *Nature Materials*, Vol. 11, May, pp.400–408.

27 Song, Y. and Dery, H. (2014) 'Magnetic field modulated resonant tunneling in ferromagnetic-insulator-nonmagnetic junctions', *arXiv*, January, pp.1–5.

28 Roy, A., Nikonov, D. and Saraswat, K. (2011) 'Electric field effects in semiconductor spin transport – a transfer matrix formalism', *Magnetics, IEEE Transactions on*, Vol. 47, October, pp.2746–2749.

29 Sears, M.R. and Saslow, W.M. (2012) 'Spin accumulation at ferromagnet/nonmagnetic material interfaces', *Phys. Rev. B*, Vol. 85, January, p. 014404.

30 V. Zayets, 'Spin and charge transport in materials with spin-dependent conductivity', *Phys. Rev. B*, Vol. 86, November, p.174415.

31 Valet, T. and Fert, A. (1993) 'Theory of the perpendicular magnetoresistance in magnetic multilayers', *Phys. Rev. B*, Vol. 48, September, pp.7099–7113,

32 Fert, A. and Jaffrès, H. (2001) 'Conditions for efficient spin injection from a ferromagnetic metal into a semiconductor', *Phys. Rev. B*, Vol. 64, October, p.184420.

33 Yu, Z.G. and Flatté, M.E. (2002) 'Spin diffusion and injection in semiconductor structures: electric field effects', *Phys. Rev. B*, Vol. 66, December, p.235302.

34 Tietze, U. and Schenk, C. (2008) *Electronic Circuits – Handbook for Design and Applications*, 2nd ed., Springer, No. 12, Berlin Heidelberg, New York.

35 Zhao, W., Torres, L., Guillemenet, Y., Cargnini, L., Lakys, Y., Klein, J., Ravelosona, D., Sassatelli, G. and Chappert, C. (2011) 'Design of MRAM based logic circuits and its applications', *ACM Great Lakes Symposium on VLSI*, pp.431–436, 2011.

36 Windbacher, T., Mahmoudi, H., Sverdlov, V. and Selberherr, S. (2013) 'Rigorous simulation study of a novelnon-volatile magnetic flip flop', *Proc. of the SISPAD*, pp.368–371.

37 Windbacher, T., Mahmoudi, H., Sverdlov, V. and Selberherr, S. (2014) *Spin Torque Magnetic Integrated Circuit*, EP13161375, Filed at: 2013-03-27, 1 October.

38 Nikonov, D., Bourianoff, G. and Ghani, T. (2011) 'Proposal of a spin torque majority gate logic', *IEEE Electron Device Lett.*, Vol. 32, No. 8, pp.1128–1130.

39 Gilbert, T. (1955) 'A lagrangian formulation of the gyromagnetic equation of the magnetization field', *Phys. Rev.*, Vol. 100, p.1243.

40 Kronmüller, H. (2007) *Handbook of Magnetism and Advanced Magnetic Materials*, Chapter General Micromagnetic Theory, John Wiley & Sons, Ltd, Hoboken, NJ, USA.

41 Slonczewski, J.C. (2005) 'Currents, torques, and polarization factors in magnetic tunnel junctions', *Phys. Rev. B*, Vol. 71, January, p.024411.

42 Xiao, J., Zangwill, A. and Stiles, M. (2004) 'Boltzmann test of Slonczewski's theory of spin-transfer torque', *Phys. Rev.*, Vol. 70, November, p.172405.

43 Sankey, J.C., Cui, Y-T., Sun, J.Z., Slonczewski, J.C., Buhrman, R.A. and Ralph, D.C. (2008) 'Measurement of the spin-transfer-torque vector in magnetic tunnel junctions', *Nature Phys.*, Vol. 4, January, pp.67–71.

44 Kubota, H., Fukushima, A., Yakushiji, K., Nagahama, T., Yuasa, S., Ando, K., Maehara, H., Nagamine, Y., Tsunekawa, K., Djayaprawira, D., Watanabe, N. and Suzuki, Y. (2008) 'Quantitative measurement of voltage dependence of spin-transfer torque in MgO-based magnetic tunnel junctions', *Nature Phys.*, Vol. 4, pp.37–41.

45 Khvalkovskiy, A.V., Zvezdin, K.A., Gorbunov, Y.V., Cros, V., Grollier, J., Fert, A. and Zvezdin, A.K. (2009) 'High domain wall velocities due to spin currents perpendicular to the plane', *Phys. Rev. Lett.*, Vol. 102, February, p.067206.

46 Miltat, J.E. and Donahue, M.J. (2007) *Handbook of Magnetism and Advanced Magnetic Materials*, Chapter Numerical Micromagnetics: Finite Difference Methods, John Wiley & Sons, Ltd, Hoboken, NJ, USA.

47 Hertel, R. (2007) *Handbook of Magnetism and Advanced Magnetic Materials*, Chapter Guided Spin Waves, John Wiley & Sons, Ltd, Hoboken, NJ, USA.

48 Windbacher, T., Mahmoudi, H., Sverdlov, V. and Selberherr, S. (2014) ‘Influence of magnetization variations in the free layer on a non-volatile magnetic flip flop’, *Proc. Intl. Conf. on Ultimate Integration on Silicon (ULIS)*, (Stockholm), April, p.4.

49 Harms, J., Ebrahimi, F., Yao, X. and Wang, J-P. (2010) ‘SPICE Macromodel of spin-torque-transfer-operated magnetic tunnel junctions’, *Electron Devices, IEEE Transactions on*, Vol. 57, June, pp.1425–1430.

50 Aharoni, A. (1998) ‘Demagnetizing factors for rectangular ferromagnetic prisms’, *J. Appl. Phys.*, Vol. 83, No. 6, pp.3432–3434.

51 Sbiaa, R., Lua, S.Y.H., Law, R., Meng, H., Lye, R. and Tan, H.K. (2011) ‘Reduction of switching current by spin transfer torque effect in perpendicular anisotropy magnetoresistive devices’, *J. Appl. Phys.*, Vol. 109, No. 7, pp.07C70-1–07C70-5.

52 Zeng, Z., Finocchio, G., Zhang, B., Amiri, P.K. Katine, J.A., Krivorotov, I.N., Huai, Y., Langer, J., Azzerboni, B., Wang, K.L. and Jiang, H. (2013) ‘Ultralow-current-density and bias-field-free spin-transfer nano-oscillator’, *Sci. Rep.*, Vol. 3, March, pp.1–5.

53 Windbacher, T., Makarov, A., Mahmoudi, H., Sverdlov, V. and Selberherr, S. (2014) ‘Novel bias-field-free spin transfer oscillator’, *J. Appl. Phys.*, Vol. 115, No. 17, pp.1–3.

54 Berkov, D. and Miltat, J. (2008) ‘Spin-torque driven magnetization dynamics: micromagnetic modeling’, *J. Magn. Magn. Mater.*, Vol. 320, No. 7, pp.1238–1259.

55 Osborn, J.A. (1945) ‘Demagnetization factors of the general ellipsoid’, *Phys. Rev.*, Vol. 67, Nos. 11–12, pp.351–357.

56 Makarov, A., Sverdlov, V. and Selberherr, S. (2013) ‘Concept of a bias-field-free spin-torque oscillator based on two MgO-MTJs’, *Solid State Devices and Materials Conference (SSDM)*, pp.796–797.